MATERIALS SCIENCE

10.1126/sciadv.1500224

Unraveling metamaterial properties in zigzag-base folded sheets

Maryam Eidini* and Glaucio H. Paulino†

Creating complex spatial objects from a flat sheet of material using origami folding techniques has attracted attention in science and engineering. In the present work, we use the geometric properties of partially folded zigzag strips to better describe the kinematics of known zigzag/herringbone-base folded sheet metamaterials such as Miura-ori. Inspired by the kinematics of a one–degree of freedom zigzag strip, we introduce a class of cellular folded mechanical metamaterials comprising different scales of zigzag strips. This class of patterns combines origami folding techniques with kirigami. Using analytical and numerical models, we study the key mechanical properties of the folded materials. We show that our class of patterns, by expanding on the design space of Miura-ori, is appropriate for a wide range of applications from mechanical metamaterials to deployable structures at small and large scales. We further show that, depending on the geometry, these materials exhibit either negative or positive in-plane Poisson's ratios. By introducing a class of zigzag-base materials in the current study, we unify the concept of in-plane Poisson's ratio for similar materials in the literature and extend it to the class of zigzag-base folded sheet materials.

INTRODUCTION

Origami, the art of paper folding, has been a substantial source of inspiration for the innovative design of mechanical metamaterials (*1*–*5*), whose material properties arise from their geometry and structural layout. Kirigami, the art of paper cutting, has been used in combination with origami to fabricate complex microstructures through microassembly (*6*) and to create three-dimensional (3D) core structures (*7*–*10*). Furthermore, rigid origami is a subset of origami structures where rigid panels (facets) are linked through perfect hinges, leading to an entirely geometric mechanism. The mathematical theory of rigid origami has been studied by various researchers (*11*–*15*). On the basis of rigid origami behavior, recent research on Miura-ori (*1*, *3*) has shown that metamaterial properties arise from its folding geometry. Miura-ori is a classic origami folding pattern whose main constituents are parallelogram facets, which are connected along fold lines. Morphology and/or mechanisms similar to those of Miura-ori naturally arise in insect wings (*16*), tree leaves (*17*), and embryonic intestines (*18*, *19*). Moreover, a self-organized wrinkling pattern of a planar stiff thin elastic film connected to a soft substrate subjected to biaxial compression (that is, a herringbone pattern) has similarities to Miura-ori (*20*–*22*), and such a herringbone pattern has been reported to correspond to the minimum energy configuration (*23*). Applications of the Miura-ori pattern range from folding of maps (*24*) to technologies such as deployable solar panels (*25*), foldcore sandwich panels (*26*, *27*), and metamaterials (*1*–*3*).

Motivated by the outstanding properties and broad range of applications of Miura-ori, we start the present study by raising a question: Can we design patterns that preserve the remarkable properties of Miura-ori and expand on its design space? To address this question, upon closer inspection of Miura-ori, we associate its kinematics with that of a one–degree of freedom (DOF) zigzag strip and present a technique to create zigzag-base mechanical metamaterials, including various scales of zigzag strips. Our method to create patterns relies on connecting zigzag strips of parallelogram facets with identical kinematics to produce one-DOF mechanism structures. Through this study, we answer the question affirmatively.

Poisson's ratio is an important material property used in the present work to create patterns and to study size changes in folded sheets. It is defined as the negative ratio of elastic extensional strain in the direction normal to the applied load to the axial extensional strain in the direction of the applied load. Most commonly, when a material is stretched in a given direction, it tends to get narrower in the direction perpendicular to the applied load. However, when stretched, materials with negative Poisson's ratio or auxetic materials expand in the direction perpendicular to the applied load. Upon bending, anticlastic (saddle-shaped) and synclastic (spherical) curvatures are observed in materials with positive and negative Poisson's ratios, respectively (*28*, *29*). On the basis of the theory of elasticity, the Poisson's ratio for thermodynamically stable isotropic linear elastic materials is bounded between −1 and 0.5 (*30*). In contrast to isotropic solids, the Poisson's ratio in anisotropic elastic materials is unrestricted ($-\infty < \upsilon < \infty$) (*31*). Folded sheets are anisotropic materials in which deformation happens as a result of folding and unfolding. Thus, in folded sheet materials (for instance in most ranges for geometric parameters of the Miura-ori folding pattern), the Poisson's ratio can assume values outside the bounds of isotropic materials (*1*, *3*).

RESULTS

Creation of patterns

In this section, we look closely at the kinematics of Miura-ori as a zigzag-base folding pattern, which provides inspiration to create a class of mechanical metamaterials. A regular Miura-ori sheet contains zigzag strips of parallelogram facets in which each unit cell can be decomposed into two V-shapes (Fig. 1A). Each V-shape includes two rigid parallelogram facets connected via a hinge along joining ridges, as shown in Fig. 1B. The Poisson's ratio considering the in-plane kinematics of a

Department of Civil and Environmental Engineering, University of Illinois at Urbana-Champaign, 205 North Mathews Avenue, Urbana, IL 61801, USA.
*Corresponding author. E-mail: eidinin1@illinois.edu
†Present address: School of Civil and Environmental Engineering, Georgia Institute of Technology, Jesse W. Mason Building, 790 Atlantic Drive NW, Atlanta, GA 30318, USA.

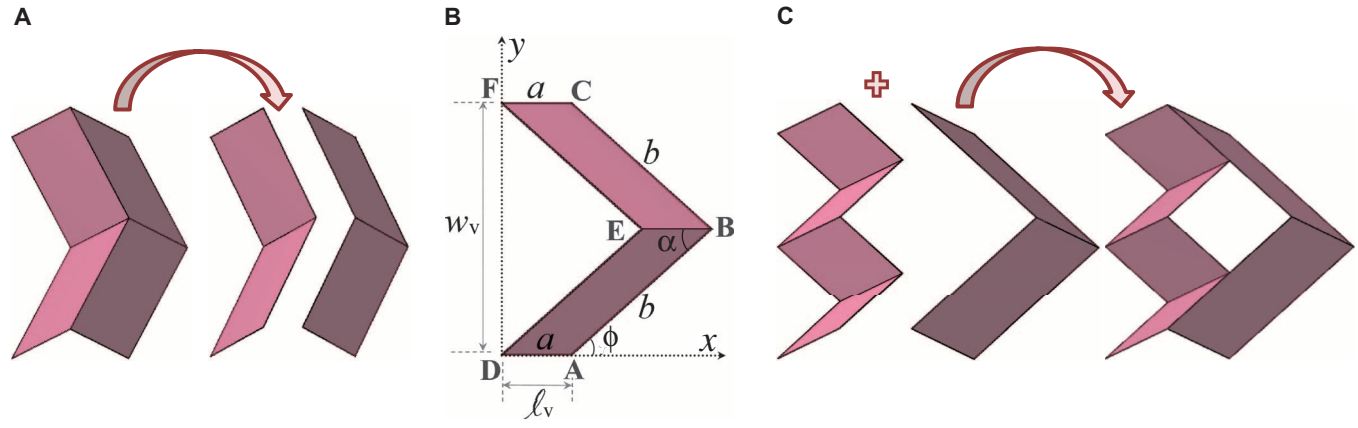

Fig. 1. From Miura-ori to zigzag-base foldable metamaterials with different scales of zigzag strips. (**A**) A Miura-ori unit cell containing two V-shapes aligned side by side, forming one concave valley and three convex mountain folds (or vice versa if the unit cell is viewed from the opposite side). (**B**) Top view of a V-shape fold including two identical parallelogram facets connected along the ridges with length *a*. Its geometry can be defined by the facet parameters *a*, *b*, and α, and by the angle ϕ ∈ [0, α]. (**C**) Two different scales of V-shapes, with the same angle ϕ, connected along joining fold lines. The length *b* of parallelogram facets in the left zigzag strip of V-shapes is half that of the strip on the right in the unit cell shown.

one-DOF V-shape (for more details, see the Supplementary Materials) is given by

$$(\upsilon_{w\ell})_V = -\frac{\varepsilon_{\ell_v}}{\varepsilon_{w_v}} = -\frac{d\ell_v/\ell_v}{dw_v/w_v} = -\tan^2\phi, \quad (1)$$

where ℓ_v is the projected length of the edges *a* in the *xy* plane and in the *x* direction, w_v is the width of the semifolded V-shape in the *xy* plane and along the *y* direction, and ϕ is the angle in the *xy* plane between the edge *b* and the *x* axis. The abovementioned expression shows that the Poisson's ratio of a V-shape is only a function of the angle ϕ. In particular, it shows that, in a unit cell containing two V-shapes arranged side by side in a crease pattern, we can scale down the length *b* of parallelogram facets to 1/*n* that of the other joining V-shape (where *n* is a positive integer) while preserving the capability of folding and unfolding. Using this insight in our current research, we create a class of zigzag-base metamaterials in which the unit cell includes two different scales of V-shapes with equivalent ϕ angles (Fig. 1C). For instance, *n* is equal to 2 for the unit cell shown in Fig. 1C. In the case of $n = 2$ from numerical models and constructed geometry, the ideal unit cell has only one planar mechanism (see Section 7-1 in the Supplementary Materials); that is, the geometry of the unit cell properly constrains the V-shapes to ideally yield a single-DOF planar mechanism. Therefore, the condition for which we have studied the kinematics of the V-shape is met.

BCH_n zigzag-base patterns

The BCH_n (Basic unit Cell with Hole) unit cell introduced in Fig. 1C is parameterized in Fig. 2A. The unit cell includes two large and 2*n* small parallelogram rigid panels joined via fold lines. For example, for the unit cell shown in Fig. 2A, *n* is equal to 2. Large values of *n*, although theoretically possible, have not been explored. For a large *n*, a zigzag strip of small parallelograms approaches a narrow strip. In the current research, we use only $n = 2$ and $n = 3$ in BCH patterns, with emphasis on BCH_2. We can define the unit cell by the geometry of parallelogram facets (with sides *a* and *b* and acute angle α ∈ [0, π/2]), and the angle ϕ ∈ [0, α], which is half the angle between the edges b_1

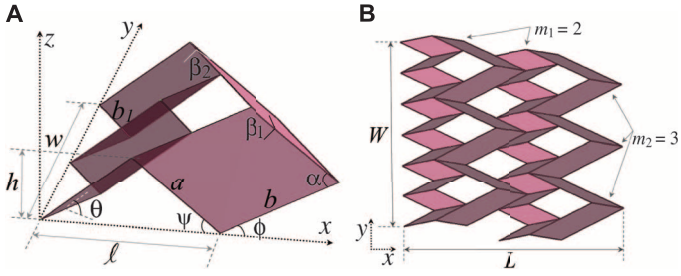

Fig. 2. Geometry of BCH_n pattern. (**A**) Geometry of the unit cell. The geometry of a BCH_n sheet can be parameterized by the geometry of parallelogram facets (*a*, *b*, and α), the half number of small parallelogram facets (*n*), and the fold angle ϕ ∈ [0, α], which is the angle between fold lines *b* and the *x* axis. Other important angles in the figure include the fold angle between the facets and the *xy* plane (that is, θ ∈ [0, π/2]), the angle between the fold lines *a* and the *x* axis (that is, ψ ∈ [0, α]), and the dihedral fold angles between parallelograms $\beta_1 \in [0, \pi]$ and $\beta_2 \in [0, \pi]$ joined along fold lines *a* and *b*, respectively. (**B**) A BCH_2 sheet with $m_1 = 2$, $m_2 = 3$, and outer dimensions *L* and *W*.

in the *xy* plane. The expressions defining the geometry of BCH_n are given by

$$w = 2b\sin\phi, \quad \ell = 2a\frac{\cos\alpha}{\cos\phi}, \quad h = a\sin\alpha\sin\theta, \quad b_1 = b/n, \quad (2)$$

where ℓ is the projected length of zigzag strips along the *x* axis in the *xy* plane (Fig. 2A). The relationship between the angle ϕ and the fold angle θ is

$$\tan\phi = \cos\theta\tan\alpha. \quad (3)$$

The outer dimensions of a regular sheet of BCH_n (Fig. 2B) are given by

$$W = m_2(2b\sin\phi), \; L = m_1\left(2a\frac{\cos\alpha}{\cos\phi} + \frac{n-1}{n}b\cos\phi\right) + \frac{1}{n}b\cos\phi. \quad (4)$$

In the relation given for the length *L*, the expression in parentheses represents the length of the repeating unit cell, and the last term (outside

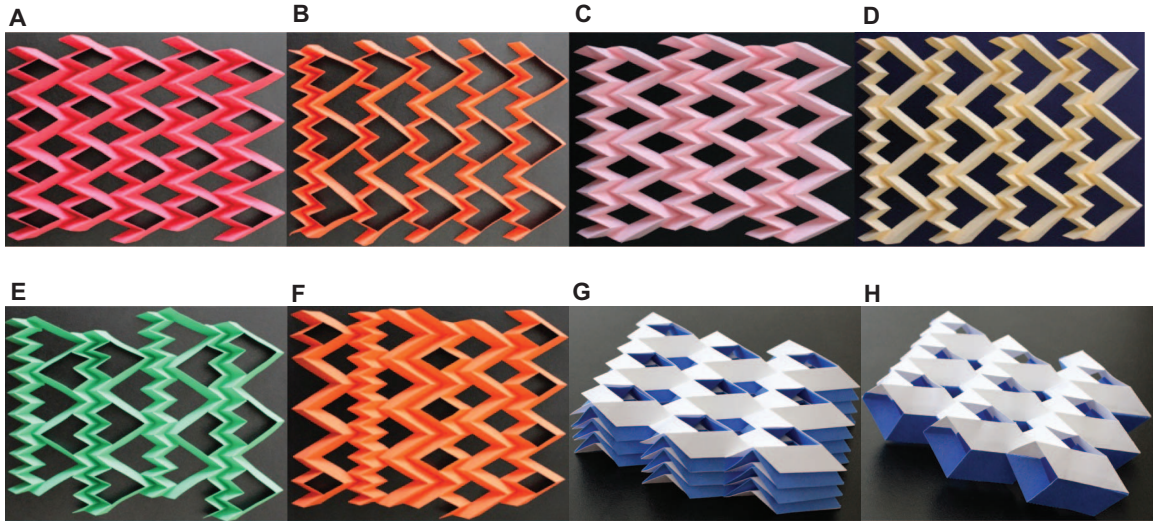

Fig. 3. Sample patterns of BCH_n and cellular folded metamaterials. (**A**) A BCH_2 sheet. (**B**) A BCH_3 sheet - adding one layer of small parallelograms to the first row reduces the DOF of the system to 1 for rigid origami behavior. (**C**) Combination of BCH_2 and layers of large and small parallelograms with the same geometries as the ones used in BCH_2. (**D**) Combination of BCH_3 and layers of large and small parallelograms with the same geometries as the ones used in BCH_3. (**E**) A BCH_3 sheet and layers of small parallelograms with the same geometries as the ones used in BCH_3. (**F**) A sheet composed of various BCH_n and Miura-ori cells with the same angle ϕ. (**G**) A stacked cellular metamaterial made from seven layers of folded sheets of BCH_2 with two different geometries. (**H**) Cellular metamaterial made from two layers of 3 × 3 sheets of BCH_2 of different heights tailored for stacking and bonded along the joining fold lines. The resulting configuration is flat-foldable in one direction.

parentheses) shows the edge effect. The second term in parentheses is related to the effect of holes in tessellation.

For rigid panels connected via hinges at fold lines, the BCH with n = 2 has only one independent DOF, on the basis of the geometry of the unit cell. In general, the number of DOF for each unit cell of BCH_n is $2n - 3$. Using at least two consecutive rows of small parallelograms, instead of one, in BCH_n (fig. S1B) decreases the DOF of BCH to 1, irrespective of the number of n (for more details, see fig. S2 and Section 7-1 in the Supplementary Materials). In addition, the patterns are rigid- and flat-foldable. Moreover, they can be folded from a flat sheet of material (that is, they are developable) (movie S1). Figure 3 presents a few configurations of the patterns.

Mechanical properties of BCH_n patterns

In the present research, we obtain the in-plane Poisson's ratio in two different ways: (i) by considering the projected lengths of zigzag strips and (ii) by considering the end-to-end dimensions of a sheet. Although the first approach is valuable to provide insights on the kinematics of a zigzag-base folded sheet such as Miura-ori and BCH_2, the latter definition can also be relevant depending on the application. To emphasize these two important concepts in relation to the folded sheet materials introduced in this work, we designate the value obtained by the first approach as υ_z and the latter as $\upsilon_{e\text{-}e}$, where the indices z and e-e stand for zigzag and end-to-end, respectively (see Fig. 4A and fig. S3). For the sheet of BCH_2 shown in Fig. 2B, ℓ and L are used to obtain υ_z and $\upsilon_{e\text{-}e}$, respectively. In fact, ℓ for a sheet is the sum of the projected lengths of zigzag strips in the xy plane and parallel to the x axis; for a sheet made of tessellations of identical BCH_2, ℓ is equal to m_1 times that of a unit cell (Fig. 4A). Alternatively, L is the end-to-end dimension of the sheet, as shown in Fig. 2B. Because the width of the sheet along the y axis is always a factor of sin ϕ, we can consider $W = w$ in both approaches. Hence, υ_z of the sheet is given by the following relation, which is equal to the kinematics of a V-shape outlined in previous sections

$$(\upsilon_{w\ell})_z = -\frac{\varepsilon_\ell}{\varepsilon_w} = -\frac{d\ell/\ell}{dw/w} = -\tan^2\phi. \quad (5)$$

Accordingly, BCH_2 and all other combined patterns of BCH with one-DOF planar mechanisms (for example, patterns shown in Fig. 3) have υ_z equal to $-\tan^2\phi$ (Fig. 4, A and B). We emphasize that the in-plane Poisson's ratio, which is obtained by considering the projected lengths of zigzag strips in the patterns, also provides an insight that components with identical υ_z can be connected to obtain a material that can freely fold and unfold (for example, Fig. 3F and movie S1). In addition, using this insight, we can create numerous configurations of metamaterials (for more details, see the Supplementary Materials).

For sheets made by tessellations of the same BCH_n (for example, Fig. 3A), $\upsilon_{e\text{-}e}$ is given by

$$(\upsilon_{WL})_{e-e} = -\frac{\varepsilon_L}{\varepsilon_W} = -\frac{dL/L}{dW/W} = -\tan^2\phi\,\frac{\kappa\,\lambda\cos\alpha - \cos^2\phi}{\kappa\,\lambda\cos\alpha + \cos^2\phi}, \quad (6)$$

with

$$\kappa = \frac{2n \cdot m_1}{m_1(n-1)+1} \quad \text{and} \quad \lambda = a/b, \quad (7)$$

in which n = 2 (n = 1 reduces to the relation for the Miura-ori sheet). Considering end-to-end dimensions, for a unit cell of BCH_2 (m_1 = 1), $\upsilon_{e\text{-}e}$ is identical to that of a Miura-ori unit cell (Fig. 4C) and is given by:

$$(\upsilon_{WL})_{e-e} = -\tan^2\phi\,\frac{2\lambda\cos\alpha - \cos^2\phi}{2\lambda\cos\alpha + \cos^2\phi}. \quad (8)$$

Therefore, unlike υ_z, which is always negative (Fig. 4B), $\upsilon_{e\text{-}e}$ can be positive for some geometric ranges (Fig. 4, C and D). Moreover, υ_z

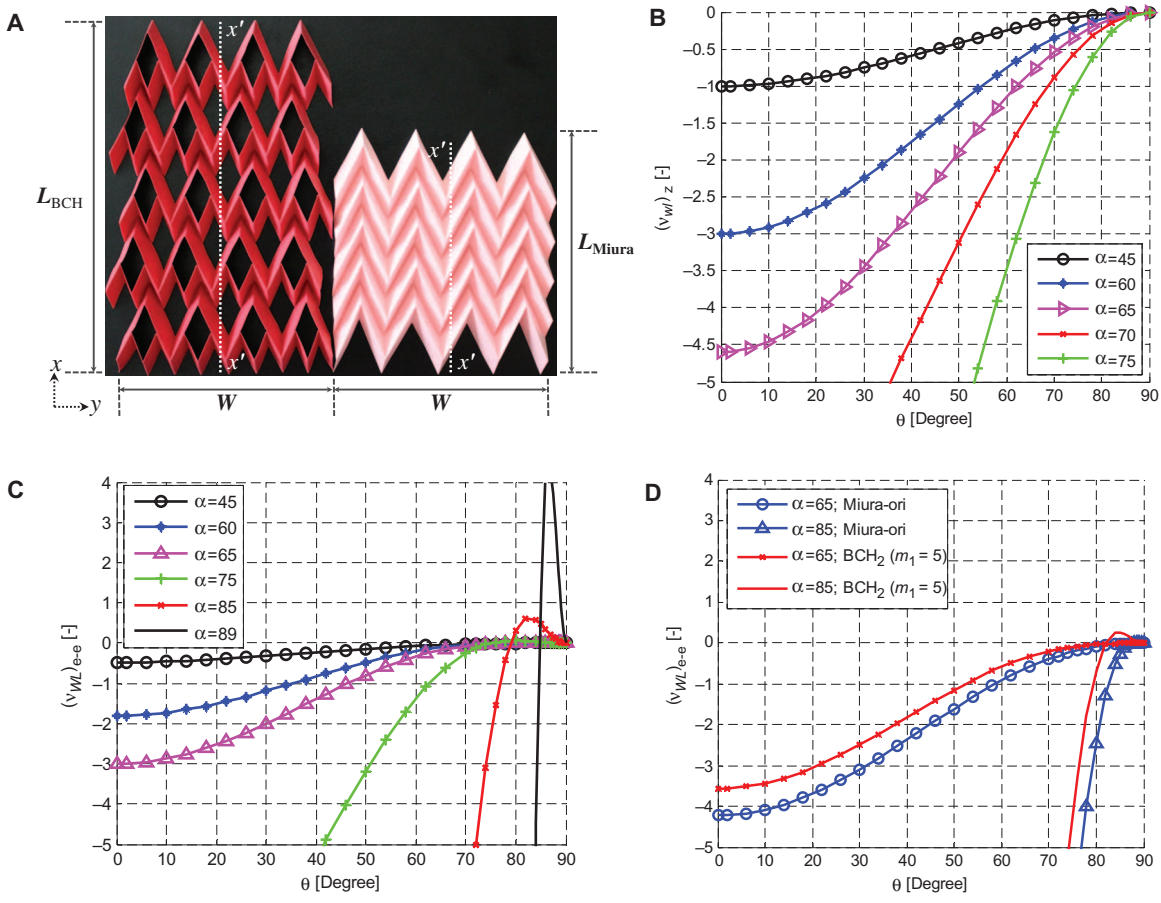

Fig. 4. In-plane Poisson's ratios of finite configurations of metamaterials. (**A**) A 5 × 4 (m_1 = 5 and m_2 = 4) BCH_2 sheet (**left**) and its corresponding Miura-ori sheet (**right**) with the same basic geometry and same amount of material. Projected lengths of zigzag strips along the *x*′–*x*′ line parallel to the *x* axis are used to obtain υ_z, and *L* is used to obtain $\upsilon_{e\text{-}e}$. Both sheets have identical υ_z but have different $\upsilon_{e\text{-}e}$. (**B**) In-plane kinematics (υ_z) of the class of metamaterials. (**C**) In-plane Poisson's ratio considering the end-to-end dimensions ($\upsilon_{e\text{-}e}$) of a single unit cell of Miura-ori and BCH_2 patterns with $a = b$. (**D**) In-plane Poisson's ratio considering the end-to-end dimensions ($\upsilon_{e\text{-}e}$) of sheets of Miura-ori and BCH_2 with m_1 = 5 and $a = b$.

is only a function of the angle ϕ, but $\upsilon_{e\text{-}e}$ can be dependent on other geometric parameters [that is, the geometry of parallelogram facets (*a*, *b*, and α), tessellations (*n* and m_1), and angle ϕ]. The Poisson's ratio considering end-to-end dimensions can be positive even for a Miura-ori unit cell (Fig. 4C). Furthermore, the shift from negative Poisson's ratio to positive Poisson's ratio in Miura-ori is only an effect of the tail (*32*), and the difference between two Poisson's ratios (that is, υ_z and $\upsilon_{e\text{-}e}$) vanishes as the length of the Miura-ori sheet approaches infinity. However, for BCH patterns, the transition to positive Poisson's ratio is primarily a result of the effect of holes in the sheets; unlike Miura-ori, the difference between these two approaches (that is, υ_z and $\upsilon_{e\text{-}e}$) does not disappear even for a BCH sheet with an infinite configuration (Fig. 5). Figure 5 presents the Poisson's ratio of a repeating unit cell of BCH_2 pattern (in an infinite tessellation) that corresponds to the following expression:

$$(\upsilon_\infty)_{e\text{-}e} = -\tan^2\phi\,\frac{4\lambda\cos\alpha - \cos^2\phi}{4\lambda\cos\alpha + \cos^2\phi}. \qquad (9)$$

From Eq. 9, $(\upsilon_\infty)_{e\text{-}e}$ for the BCH_2 sheet is positive if $4\lambda\cos\alpha < \cos^2\phi$ and negative if $4\lambda\cos\alpha > \cos^2\phi$.

Analogous to the Miura-ori sheet (*1*), similar BCH sheets having the same υ_z can be designed for stacking and attached together along joining fold lines to form cellular folded metamaterials capable of folding freely (Fig. 3, G and H, and movie S2). The BCH sheets tailored for stacking have identical $\upsilon_{e\text{-}e}$ (for more details, see the Supplementary Materials).

Considering that the facets are rigid and connected via elastic rotational springs along the fold lines, we obtain measures of the planar stretching stiffness of BCH_2 in the *x* and *y* directions (fig. S5) and compare the results with their corresponding values for the Miura-ori cell. From Fig. 6, we infer that, depending on the geometry and considering the same amount of material (compare Fig. 2A with fig. S4), BCH_2 can be stiffer or more flexible than its corresponding Miura-ori cell (for more details, see the Supplementary Materials).

Simple experimental observations show that these folded sheets exhibit, similarly to the Miura-ori pattern, an anticlastic (saddle-shaped) curvature upon bending (Fig. 7A, figs. S6 to S8, and movie S3), which is a curvature adopted by conventional materials with positive out-of-plane Poisson's ratio (*29*). This positional semiauxetic behavior has been observed in "antitrichiral" honeycomb (*33*), auxetic composite laminates (*34*), and other patterns of folded sheets made of conventional materials (*1*, *3*, *28*).

We also investigate the effects of geometry and material properties on the global behavior of folded sheets using the bar-framework numerical approach described by Schenk and Guest (*1*). By considering the bending stiffness of the facets and fold lines (K_{facet} and K_{fold}, respectively), we study the modal responses of folded shells by changing the ratio of K_{facet} to K_{fold}. For the BCH_2 pattern shown in Fig. 7, twisting and bending modes are the predominant behaviors over a range of K_{facet}/K_{fold} and associated geometries (Fig. 7, B and C), similar to a regular Miura-ori sheet (*28*). Furthermore, the saddle-shaped bending mode obtained from an eigenvalue analysis of the patterns further confirms that Poisson's ratio becomes positive upon bending (*29*). The results show that for large values of K_{facet}/K_{fold}, the first softest eigenmode represents a rigid origami behavior (Fig. 7D). The results of the stiffness analysis of several other patterns from the class of metamaterials show similar behaviors (figs. S6 to S8).

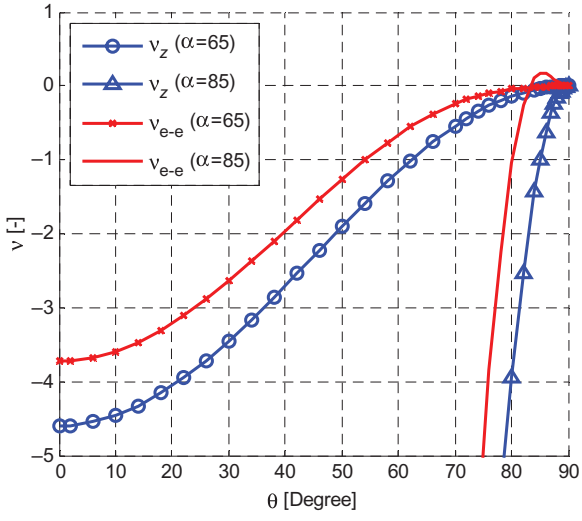

Fig. 5. In-plane Poisson's ratio of a BCH_2 sheet with infinite configuration. Poisson's ratio obtained by considering the projected length of zigzag strips υ_z versus Poisson's ratio considering the end-to-end dimensions of the sheet when the sheet size approaches infinity, $\upsilon_{e\text{-}e}$ ($a = b$ and $m_1 \rightarrow \infty$). The latter is equivalent to the Poisson's ratio of a repeating unit cell of BCH_2 in an infinite tessellation. Contrary to Miura-ori, the transition to a positive Poisson's ratio is present with an infinite configuration of the BCH_2 sheet.

DISCUSSION

Most research studies on origami-inspired materials rely on known patterns, especially on Miura-ori (that is, a classic origami pattern with outstanding properties and a wide range of applications). In this study, we have created the BCH_2 pattern among other combined patterns and have shown that the pattern has properties as remarkable as those of Miura-ori. We summarize the significant outcomes of the current research in Fig. 8 and discuss in the following section.

We have used the concept of the in-plane Poisson's ratio, a key material property in the present study, in two different contexts (see table S1):

• First, to describe the kinematics of and to create a class of one-DOF zigzag-base mechanical metamaterials: Poisson's ratio is obtained by considering the projected lengths of zigzag strips (that is υ_z), and the value is always equal to $-\tan^2 \phi$. The value obtained this way is an inherent property of the class of one-DOF zigzag-base folded sheets and is related to the foldability of the class of metamaterials. Hence, the concept provides insight into the creation of zigzag-base foldable materials. The value (that is, $-\tan^2 \phi$) has been associated with the Poisson's ratio of the Miura-ori sheet (*1*) to describe the stacking of Miura-ori in the literature (*1*). However, in the present work, after explicitly associating the value with that of a one-DOF zigzag strip (Fig. 1), we have scaled down the width of one joining zigzag strip in the unit cell and have created BCH patterns containing various scales of zigzag strips. Accordingly, the present study extends the kinematics of Miura-ori to that of a class of one-DOF zigzag-base folded sheet metamaterials. In other words, our work shows that all one-DOF zigzag-base folded metamaterials (Fig. 3) have identical kinematics when the angle ϕ is the same.

• Second, to study size changes in the folded metamaterials introduced in this work: Poisson's ratio is obtained by considering the end-to-end dimensions of a sheet, $\upsilon_{e\text{-}e}$. This definition captures size changes in a finite sheet (Fig. 4) and in a repeating unit cell (in an infinite configuration) of a regular sheet (for example, regular BCH_2; Fig. 5). Moreover, it is applicable to irregular sheets, such as that shown in Fig. 3F.

Because the recent literature on the topic had differing evaluations of Poisson's ratio (*1*, *3*, *32*), this study further clarifies the issue and unifies the concepts by introducing a class of zigzag-base folded sheet materials. For the Miura-ori sheet, the Poisson's ratio of a repeating unit cell is equal to υ_z. Hence, the value given in (*1*, *3*) presents the kinematics

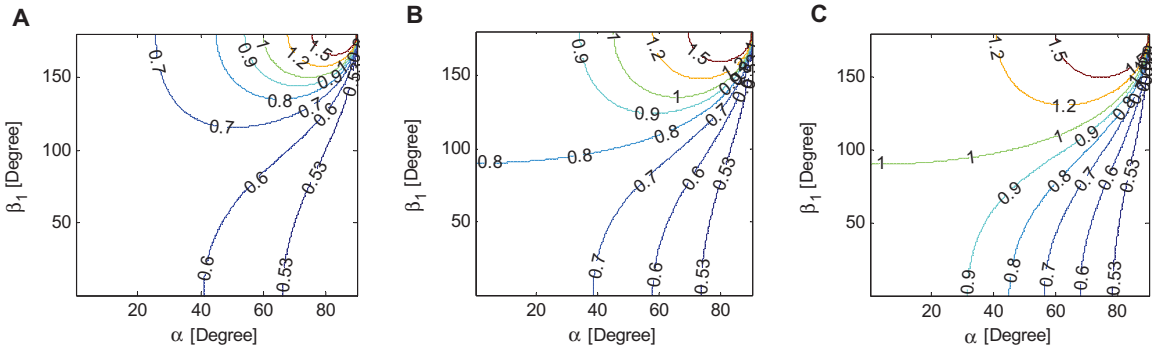

Fig. 6. Ratio of the in-plane stiffness of a Miura-ori cell to the in-plane stiffness of BCH_2 in the *x* and *y* directions. The results show that, depending on the geometry and considering the same amount of material, BCH_2 can be stiffer or more flexible than its corresponding Miura-ori cell in the *x* and *y* directions. (**A**) $a/b = 2$. (**B**) $a/b = 1$. (**C**) $a/b = 1/2$.

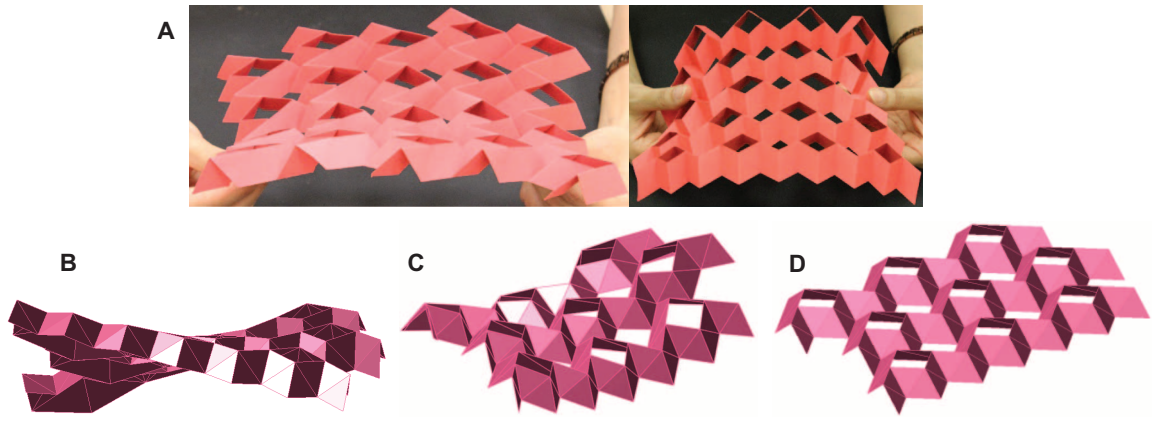

Fig. 7. Behavior of a BCH_2 sheet upon bending and results of the eigenvalue analysis of a 3 × 3 BCH_2 pattern. (**A**) A BCH_2 sheet deforms into a saddle shape upon bending (that is, a typical behavior seen in materials with a positive out-of-plane Poisson's ratio). (**B**) Twisting deformation, (**C**) saddle-shaped deformation, and (**D**) rigid origami behavior (planar mechanism) of a 3 × 3 pattern of BCH_2 ($a = 1$, $b = 2$, and $\alpha = 60°$). Twisting and saddle-shaped deformations are the softest modes observed for a wide range of material properties and geometries. For large values of K_{facet}/K_{fold}, rigid origami behavior (planar mechanism) is simulated.

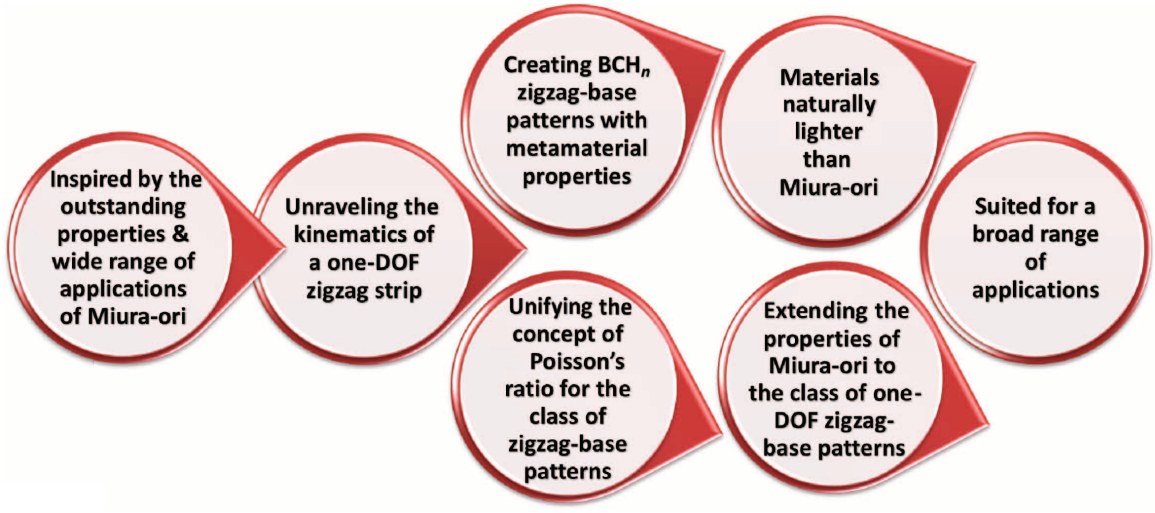

Fig. 8. Outcomes of the current study. Inspired by Miura-ori to create BCH_n zigzag-base patterns with a broad range of applications.

of the Miura-ori sheet and the size changes in a repeating unit cell of Miura-ori. Thus, considering the end-to-end dimensions of a finite Miura-ori sheet is simply capturing the edge effect (*32*) (that is, the last term given in Eq. 4 for L). However, for the BCH_2 pattern, the Poisson's ratio of a repeating unit cell is not equal to υ_z and assumes negative and positive values because of the presence of holes in the pattern (Fig. 5). Therefore, our study shows that considering the end-to-end configurations of the BCH_2 pattern is mainly capturing the effect of holes on Poisson's ratio (that is, the second term in parentheses in Eq. 4 for L).

We have also shown that the BCH_n and combined patterns introduced in this work have metamaterial properties arising from their tunable geometric configurations. An appealing feature of these patterns is that they display properties similar to those of Miura-ori; however, the presence of different scales of zigzag strips and the existence of holes make the BCH_n patterns unique (for example, Fig. 4A). In addition, the fact that the mechanical properties of BCH_n differ from those of Miura-ori (for example, Figs. 4D, 5, and 6) offers avenues to explore alternative materials and structures for specific performance/applications of the Miura-ori pattern, for which there is a surge of research interest. On the other hand, the present technology requires lighter and more customizable structures and materials. Combining cellular BCH_n patterns with Miura-ori provides an augmented design space for tailored engineering design of materials and structures. Consequently, the availability of large design motifs can be advantageous, for instance, in dynamic architectural façades where the placement of holes in patterns can be controlled to either allow light in the interior of buildings or promote shading when desirable.

In summary, the remarkable properties of the patterns (specifically of the BCH_2 pattern), such as rigid foldability, flat foldability, and single DOF, as well as numerous possible combinations of the patterns, make them well suited for a broad range of applications, including kinetic and deployable structures [for example, solar sails (*25*)], light cellular foldcore sandwich panels (*26*, *27*), 3D tunable folded

cellular metamaterials (*1*, *5*, *35*), energy-absorbing devices (*36*), foldable robots (*37*), and auxetic materials (*29*, *30*). In all these applications, scalability is an attractive feature of the BCH_n pattern and of other combined patterns because of their inherent geometric properties.

MATERIALS AND METHODS

To experimentally assess the mechanical behavior of origami-inspired patterns, we fabricated samples from various types of materials, including paper (20, 24, and 28 lb), construction paper (76 lb), and cardstock (110 lb). To create holes and pattern creases, we used an electronic cutter. We first designed the patterns and then converted them into a vector format appropriate for electronic cutting. The crease lines were perforated using a dash-and-gap style. After patterning, we manually folded the sheets along the fold lines constituting the mountains and valleys of folded sheets. We numerically verified the observed behavior of the materials using stiffness analysis over a broad range of materials, including rigid panels connected via frictionless hinges.

SUPPLEMENTARY MATERIALS

Supplementary material for this article is available at http://advances.sciencemag.org/cgi/content/full/1/8/e1500224/DC1

Supplementary text

Fig. S1. BCH_2, BCH_3, and their combinations with rows of small and/or large parallelograms.

Fig. S2. Constrained DOF by implicit formation of the structure of the Miura-ori unit cell between adjoining unit cells of BCH_2 and BCH_3 in the pattern.

Fig. S3. Concept of Poisson's ratio considering end-to-end dimensions.

Fig. S4. Geometry of a Miura-ori cell.

Fig. S5. In-plane stiffness for BCH_2 with $a = b = 1$.

Fig. S6. Behavior of a BCH_3 sheet upon bending and results of the eigenvalue analysis of a 3×3 pattern of BCH_3.

Fig. S7. Behavior of a sheet of the pattern shown in Fig. 3C upon bending and results of the eigenvalue analysis of a 2×3 sheet of the pattern.

Fig. S8. Behavior of a sheet of the pattern shown in Fig. 3D upon bending and results of the eigenvalue analysis of a 2×3 sheet of the pattern.

Table S1. Main points of the in-plane Poisson's ratio of the class of zigzag-base folded metamaterials.

Movie S1. In-plane behavior of the patterns.

Movie S2. A cellular folded metamaterial made by stacking seven layers of a 3×3 sheet of BCH_2 pattern with two different geometries.

Movie S3. Out-of-plane behavior of the patterns.

Reference (*38*)

REFERENCES AND NOTES

1. M. Schenk, S. D. Guest, Geometry of Miura-folded metamaterials. *Proc. Natl. Acad. Sci. U.S.A.* **110**, 3276–3281 (2013).
2. J. L. Silverberg, A. A. Evans, L. McLeod, R. C. Hayward, T. Hull, C. D. Santangelo, I. Cohen, Using origami design principles to fold reprogrammable mechanical metamaterials. *Science* **345**, 647–650 (2014).
3. Z. Y. Wei, Z. V. Guo, L. Dudte, H. Y. Liang, L. Mahadevan, Geometric mechanics of periodic pleated origami. *Phys. Rev. Lett.* **110**, 215501 (2013).
4. A. Norman, K. Seffen, S. D. Guest, Morphing of curved corrugated shells. *Int. J. Solids Struct.* **46**, 1624–1633 (2009).
5. T. Tachi, K. Miura, Rigid-foldable cylinders and cells. *J. Int. Assoc. Shell Spat. Struct.* **53**, 217–226 (2012).
6. N. Bassik, G. M. Stern, D. H. Gracias, Microassembly based on hands free origami with bidirectional curvature. *Appl. Phys. Lett.* **95**, 091901 (2009).
7. T. Nojima, K. Saito, Development of newly designed ultra-light core structures. *JSME Int. J., Ser. A* **49**, 38–42 (2006).
8. K. Saito, F. Agnese, F. Scarpa, A cellular kirigami morphing wingbox concept. *J. Intell. Mater. Syst. Struct.* **22**, 935–944 (2011).
9. F. Scarpa, M. Ouisse, M. Collet, K. Saito, Kirigami auxetic pyramidal core: Mechanical properties and wave propagation analysis in damped lattice. *J. Vib. Acoust.* **135**, 041001 (2013).
10. Y. Hou, R. Neville, F. Scarpa, C. Remillat, B. Gu, M. Ruzzene, Graded conventional-auxetic Kirigami sandwich structures: Flatwise compression and edgewise loading. *Compos. Part B: Eng.* **59**, 33–42 (2014).
11. D. A. Huffman, Curvature and creases: A primer on paper. *IEEE Trans. Comput.* **25**, 1010–1019 (1976).
12. K. Miura, A note on intrinsic geometry of origami. *Origami* **1**, 239–249 (1989).
13. T. Hull, *Project Origami: Activities for Exploring Mathematics* (A. K. Peters, Wellesley, MA, 2006).
14. S.-M. Belcastro, T. C. Hull, Modelling the folding of paper into three dimensions using affine transformations. *Linear Algebra Appl.* **348**, 273–282 (2002).
15. T. Tachi, Simulation of rigid origami. *Origami* **4**, 175–187 (2009).
16. F. Haas, R. J. Wootton, Two basic mechanisms in insect wing folding. *Proc. R. Soc. Lond. B Biol. Sci.* **263**, 1651 (1996).
17. H. Kobayashi, B. Kresling, J. Vincent, The geometry of unfolding tree leaves. *Proc. R. Soc. Lond. B Biol. Sci.* **265**, 147 (1998).
18. M. Ben Amar, F. Jia, Anisotropic growth shapes intestinal tissues during embryogenesis. *Proc. Natl. Acad. Sci. U.S.A.* **110**, 10525–10530 (2013).
19. A. E. Shyer, T. Tallinen, N. L. Nerurkar, Z. Wei, E. S. Gil, D. L. Kaplan, C. J. Tabin, L. Mahadevan, Villification: How the gut gets its villi. *Science* **342**, 212–218 (2013).
20. L. Mahadevan, S. Rica, Self-organized origami. *Science* **307**, 1740 (2005).
21. B. Audolya, A. Boudaoud, Buckling of a stiff film bound to a compliant substrate—Part III: Herringbone solutions at large buckling parameter. *J. Mech. Phys. Solids* **56**, 2444–2458 (2008).
22. K. Miura, The science of Miura-ori: A review. *Origami* **4**, 87–99 (2009).
23. X. Chen, J. W. Hutchinson, Herringbone buckling patterns of compressed thin films on compliant substrates. *J. Appl. Mech.* **71**, 597–603 (2004).
24. K. Miura, Map fold a la Miura style, its physical characteristics and application to the space science, in *Research of Pattern Formation*, R. Takaki, Ed. (KTK Scientific Publishers, Tokyo, Japan, 1994), pp. 77–90.
25. K. Miura, Method of packaging and deployment of large membranes in space. *Inst. Space Astronautical Sci. Univ. Tokyo Rep.* **618**, 1–9 (1985).
26. K. Miura, Zeta-core sandwich—Its concept and realization. *Inst. Space Aeronaut. Sci. Univ. Tokyo Rep.* **618**, 137–164 (1972).
27. S. Heimbs, Foldcore sandwich structures and their impact behaviour: An overview, in *Dynamic Failure of Composite and Sandwich Structures* (Springer, Netherlands, 2013), pp. 491–544.
28. M. Schenk, S. D. Guest, Origami folding: A structural engineering approach. *Origami* **5**, 291–304 (2011).
29. A. Alderson, K. L. Alderson, Auxetic materials. *Proc. IMechE J. Aerospace Eng.* **221**, 565–575 (2007).
30. R. Lakes, Foam structures with a negative Poisson's ratio. *Science* **235**, 1038–1040 (1987).
31. T. C. T. Ting, T. Chen, Poisson's ratio for anisotropic elastic materials can have no bounds. *Q. J. Mech. Appl. Math* **58**, 73–82 (2005).
32. C. Lv, D. Krishnaraju, G. Konjevod, H. Yu, H. Jiang, Origami based mechanical metamaterials. *Sci. Rep.* **4**, 5979 (2014).
33. A. Alderson, K. L. Alderson, G. Chirima, N. Ravirala, K. M. Zied, The in-plane linear elastic constants and out-of-plane bending of 3-coordinated ligament and cylinder-ligament honeycombs. *Compos. Sci. Technol.* **70**, 1034–1041 (2010).
34. T.-C. Lim, On simultaneous positive and negative Poisson's ratio laminates. *Phys. Status Solidi B* **244**, 910–918 (2007).
35. K. C. Cheung, T. Tachi, S. Calisch, K. Miura, Origami interleaved tube cellular materials. *Smart Mater. Struct.* **23**, 094012 (2014).
36. M. Schenk, S. D. Guest, G. J. McShane, Novel stacked folded cores for blast-resistant sandwich beams. *Int. J. Solids Struct.* **51**, 4196–4214 (2014).
37. S. Felton, M. Tolley, E. Demaine, D. Rus, R. Wood, A method for building self-folding machines. *Science* **345**, 644–646 (2014).
38. W. McGuire, R. H. Gallagher, R. D. Ziemian, *Matrix Structural Analysis* (Wiley, New York, ed. 2, 2000).

Funding: The current research was partially funded by the Department of Civil and Environmental Engineering of the University of Illinois at Urbana-Champaign. **Author contributions:** M.E. and G.H.P. designed the study and wrote the manuscript. M.E. performed the analyses. **Competing interests:** The authors declare that they have no competing interests.

Submitted 24 February 2015
Accepted 16 July 2015
Published 18 September 2015
10.1126/sciadv.1500224

Citation: M. Eidini, G. H. Paulino, Unraveling metamaterial properties in zigzag-base folded sheets. *Sci. Adv.* **1**, e1500224 (2015).

ScienceAdvances
AAAS

Unraveling metamaterial properties in zigzag-base folded sheets

Maryam Eidini and Glaucio H. Paulino (September 18, 2015)
Sci Adv 2015, 1:.
doi: 10.1126/sciadv.1500224